From sintering to chemical durability impact of the cationic homogeneity on the (Th,U)O2 ceramics lifecycle

Laurent Claparede, Nicolas Clavier, A. Mesbah, F. Tocino, Stephanie Szenknect, N. Dacheux

▶ **To cite this version:**

Laurent Claparede, Nicolas Clavier, A. Mesbah, F. Tocino, Stephanie Szenknect, et al.. From sintering to chemical durability impact of the cationic homogeneity on the (Th,U)O2 ceramics lifecycle. Journal of Nuclear Materials, 2018. ⟨hal-02339642⟩

HAL Id: hal-02339642

https://hal.science/hal-02339642v1

Submitted on 4 Nov 2019

HAL is a multi-disciplinary open access archive for the deposit and dissemination of scientific research documents, whether they are published or not. The documents may come from teaching and research institutions in France or abroad, or from public or private research centers.

L'archive ouverte pluridisciplinaire **HAL**, est destinée au dépôt et à la diffusion de documents scientifiques de niveau recherche, publiés ou non, émanant des établissements d'enseignement et de recherche français ou étrangers, des laboratoires publics ou privés.

HAL Authorization

From sintering to chemical durability : impact of the cationic homogeneity on the (Th,U)O_2 ceramics lifecycle

Laurent Claparede, [†,*] Nicolas Clavier, [†,*] Adel Mesbah, [†] Florent Tocino, [†] Stéphanie Szenknect, [†] and Nicolas Dacheux [†]

[†] ICSM, CEA, CNRS, ENSCM, Univ Montpellier, Site de Marcoule – Bât. 426, 30207 Bagnols-sur-Cèze, France

Abstract:

In order to study the effects of the cationic distribution homogeneity on the life cycle of $Th_{1-x}U_xO_2$ ceramics, including sintering and reprocessing (dissolution) steps, five different ways of preparation were set up, going from the most homogeneous solid solutions obtained through oxalic co-precipitation to a mechanical mixture of the parent oxides. Dilatometric experiments evidenced the better sintering capacity for the most homogenous compounds obtained through wet chemistry methods while dry chemistry routes led to poor density values (between 80 and 90 %TD). However, the introduction of additional mechanical grinding step prior the sintering of the powders systematically led to the homogenization of the systems. Improved homogeneity also provide a better chemical durability associated with the congruent dissolution of thorium and uranium in solution during dissolution tests of $Th_{0.5}U_{0.5}O_2$ samples. Conversely, heterogeneous samples led to incongruent behaviors that can be smoothed by introducing a grinding step prior the preparation of sintered samples. Since the impact of the cationic distribution homogeneity must be followed carefully during the study of the solid/solution interface evolution, in operando observations of evolving solid-solution interface by ESEM were performed during dissolution. They allowed imaging the preferential dissolution of uranium enriched zones and confirmed the important role of chemical heterogeneities present at the interface.

I. INTRODUCTION

Mixed actinide dioxides are currently used as fuels in Pressurized Water Reactors (PWR) and also stand as potential candidates for several Gen IV concepts including Sodium-cooled Fast Reactor (SFR) or Gas-cooled Fast Reactor (GFR) [1, 2]. In this field, the reprocessing of minor actinides coming from nuclear spent fuel into mixed-oxide fuels or in UO_2-based blankets surrounding the core is often considered [3]. In a similar way, the preparation of Pu- and U- bearing ThO_2 samples was already described in literature and proposed as advanced fuel materials [4-7]. Indeed, thoria (ThO_2) presents a great interest for its potential use in nuclear energy applications, as ^{232}Th can be used to produce ^{233}Th ($T_{1/2}$ = 21.83 minutes) by neutron capture then ^{233}Pa ($T_{1/2}$ = 27 days) and finally ^{233}U (fissile isotope, $T_{1/2}$ = 159200 years) by two successive β^- decays.

Mixed actinide dioxides were usually prepared through powder metallurgy methods (i.e. mechanical mixture of parent oxides) which could result in some heterogeneities in the cationic distribution within the material [8]. As a consequence, wet chemistry methods were investigated with the aim to monitor the physico-chemical properties of the final oxides from the synthesis step. These processes are mainly based on the precipitation of crystallized precursors [9] such as carbonates, nitrates, hydroxides or oxalates [10-13]. These latter remained probably the most frequently cited in the literature as they provide a rapid and quantitative precipitation of actinides from solution. Also, they led to the formation of homogenous solid solutions which ensure the homogeneity of the cation distribution at the molecular scale. This enhanced homogeneity is then thought to be one of the main factors leading to the improvement of several properties of interest of the system, including sintering capability of the mixed oxide powder obtained after thermal conversion, or chemical durability of the final ceramics [14, 15].

Several authors already underlined the importance of homogeneity during the sintering of actinide mixed oxides. Indeed, the densification of the samples mainly proceeds through solid-state diffusion. Starting with heterogeneous powders generally delays the sintering process since the formation of an homogenous solid solutions is the first mechanism triggered [16-18]. Also, important differences in the diffusion coefficients of the cations considered can led to the formation of porosity, due to the well-known Kirkendall effect [19, 20]. In this context, the initial co-precipitation of actinide cations, particularly as oxalate precursors, was found to provide homogenous oxide powders after heat treatment, which further present improved sintering capability; the temperature needed to achieve a complete densification

being lowered by 100 to 200°C compared to powder metallurgy processes [15]. Nevertheless, if this effect was systematically correlated to the homogeneity of the cation distribution in the starting powder, no specific study was undertaken on this point to our knowledge.

Similarly, the multiparametric study of the dissolution of $Th_{1-x}U_xO_2$ solid solutions was recently examined by varying conventional parameters such as temperature, chemical composition or leachate acidity [14, 21-23]. However, the consequences of the physico-chemical modifications (including morphology) induced by the chemical way of synthesis considered on the chemical durability were only recently evocated [11, 12, 24] while they appear as key parameters either for the understanding of the reprocessing operations or for the long-term storage of spent nuclear fuels.

In this context, this work is focused on the effects of the cationic distribution on the life cycle of $Th_{1-x}U_xO_2$ ceramics, including sintering and reprocessing (dissolution) steps. Thorium-uranium-(IV) mixed dioxides were selected as a simplified model of other tetravalent actinides oxides (such as uranium, neptunium, plutonium). Five different ways of preparation were then set up in order to prepare $Th_{1-x}U_xO_2$ ceramics with different characteristics in terms of cationic distribution, going from the most homogeneous solid solutions obtained through oxalic co-precipitation to a mechanical mixture of both end-members. The various powders obtained were further characterized by the means of SEM and XRD to evidence the microstructural characteristics of the different samples. Their sintering capability was then evaluated through a dilatometric study combined with SEM-EDX mapping analysis. Finally, the chemical durability of the samples was determined during dissolution tests in highly acid media while *in operando* observations of the solid/solution interface evolution were performed by ESEM during dissolution.

II. EXPERIMENTAL SECTION

2.1. Synthesis and thermal conversion

Caution! uranium and thorium are natural radioelements, more often involving α-emitters and as such are considered a health risk. Their use requires appropriate infrastructure and personnel training regarding the handling of radioactive materials.

The Following materials were used to perform the synthesis and the dissolution tests: depleted U (kindly supplied by CETAMA, France), $Th(NO_3)_4.4\text{-}5\ H_2O$, $H_2C_2O_4$, HCl, HNO_3 (Sigma Aldrich). The actinides solutions were prepared by dissolving metallic U or Th salt in hydrochloric acid (6M). The final concentration of cations in each solution was about 0.5M and was accurately determined by Inductively-Coupled Plasma Atomic Emission Spectroscopy (ICP-AES, Spectro Arcos) or Photon-Electron Rejecting Alpha Liquid Scintillation (PERALS, Ametek) measurements.

In order to prepare a set of $Th_{0.5}U_{0.5}O_2$ oxides exhibiting various homogeneities in the distribution between uranium and thorium, five methods were set up:

I. First, an homogenous solid solution $Th_{0.5}U_{0.5}(C_2O_4)_2.2H_2O$ was prepared under mild hydrothermal conditions (130 °C, 7 days) in application of the protocol proposed by Clavier *et al.*[15, 25] which leads to large single crystals. The resulting oxalate precipitate was further heated at 500°C under Ar/H_2 4% to yield the final $Th_{0.5}U_{0.5}O_2$ sample.

II. In order to benefit from the good homogeneity provided by the oxalic co-precipitation, but with a different morphology, a distinct $Th_{0.5}U_{0.5}(C_2O_4)_2.2H_2O$ mixed oxalate was prepared by direct co-precipitation in an open vessel at 60°C. In this case, the acidic solutions containing the cations were first mixed together in the desired ratio, then poured into a large excess of oxalic acid. The precipitate was rapidly formed and was further separated by centrifugation, washed and dried. Afterwards, the obtained powder was converted to $Th_{0.5}U_{0.5}O_2$ by thermal treatment at 500°C.

III. The first of the “heterogeneous” samples was prepared by grinding manually in an agate mortar, an equimolar mixture of single phase $Th(C_2O_4)_2.2H_2O$ and $U(C_2O_4)_2.2H_2O$ in an equivalent molar ratio. It was then heated at 500°C to obtain

the oxide compound.

IV. In a modification of the protocol described above, both oxalate precursors were converted into ThO_2 and UO_2 by heating at 500°C, then mixed thoroughly in a mortar.

V. Lastly, protocol IV was slightly modified. In this case, both oxalate precursors were converted into ThO_2 and UO_2 by heating at 1000°C, then mixed thoroughly in a mortar.

Moreover, it is important to note that a second set of materials was prepared using the same five protocols described above but with the addition of a mechanical grinding step (30 Hz, 30 min.) within a zirconia jar prior the final treatment at high temperature. Such modification aimed to evaluate how the heterogeneities inherited from the preparation methods can be hindered by an additional grinding step performed afterwards.

2.2. Powders characterization and sintering

PXRD. The powdered samples obtained either after precipitation of oxalate precursors or after their thermal conversion into oxides were characterized by powder X-ray diffraction (PXRD) using a Bruker D8 diffractometer equipped with a Lynx-eye detector and Cu $K\alpha_{1,2}$ (λ = 1.54184 Å) adopting the reflection mode (parallel beam). PXRD patterns were recorded at room temperature in dedicated sealed sample holders in order to avoid radioactive contamination in the $5° \leq 2\theta \leq 120°$ angular range, with a step size $\Delta(2\theta)$ of 0.03° and an average total counting time of about 3 hours per sample.

The collected PXRD patterns were then refined by the Rietveld method using the Fullprof_suite program [26] in order to evaluate the average crystallite size (i.e. average length of the coherent domains). Pure silicon was used as external standard to extract the instrumental function. For each refined pattern, the following parameters were allowed to vary: zero shift, unit cell parameters, scale factors, global thermal displacement. Moreover, the modelling of the intrinsic microstructure parameters was performed for each phase by applying an anisotropic size model.

SEM. Morphological characterization of the samples was performed using a FEI Quanta 200 environmental scanning electron microscope equipped with a backscattered

electron detector (BSED) or a secondary electron detector (SE) in vacuum conditions with an acceleration voltage of 25 kV. Samples were always directly analysed without any additional preparation step such as metallization.

SEM micrographs recorded at low magnification were first used to evaluate the initial specific surface area (S_{SA} in $m^2.g^{-1}$) of the pellets using the SESAM (Study of Evolving Surface Area by Microscopy) method [27, 28]. With this aim, 5 images of 92 µm× 62 µm were binarized using the FiJi software to determine the surface area of the pores visible in the investigated domains. The distribution of the pore diameter was evaluated from these images using the "analyse particles" plugin implemented in the FiJi software. Then, the surface area associated to the pores was obtained assuming that the pore size distribution of the analysed domain was representative of the whole sample and that the pores were cylindrical. The determined surface area of the pores were then weighted by the fraction of open porosity deduced from apparent and pycnometric densities and the resulting surface was divided by the mass of the sample to calculate the specific surface area. For each sample, an average value of the specific surface area was deduced from the analysis of the 5 images recorded at low magnification.

Additionally, X-EDS mapping of the surface of sintered samples was performed in order to evaluate the homogeneity of the cations distribution within the pellets. Sintered samples were first polished up to a mirror grade. A selected area of about 150×100 µm was then analysed during 4 hours. These conditions ensured reliable counting statistics associated to an important number of data points (750 000) which can be considered as representative of the whole pellet surface. Also, the counting rate was kept constant for all the zones analysed, in order to avoid any analytical bias during the data analysis.

Sintering. The obtained powders were shaped by uniaxial pressing (500 MPa) in a tungsten carbide die as cylindrical green pellets of 5 mm in diameter and about 1 to 2 mm thickness. The sintering of these compacts was further monitored by dilatometric measurements using a Setaram Setsys Evolution apparatus. Heating treatments were performed under Ar flux up to 1500°C with a rate of $10°C.min^{-1}$. An isothermal plateau was then applied during 8 hours before the sample was cooled down to room temperature at $30°C.min^{-1}$. The resulting dense pellets were further investigated by the means of SEM (see above) and geometrical density measurements using a precision calliper.

2.3. Dissolution experiments

The leaching experiments were carried out using high-density polytetrafluroethylene (PTFE) vessels (volume of 25 mL) in order to avoid any adsorption of released elements on the containers walls. Dissolution tests were first performed under static conditions : pellets of around 200 mg were put in contact with 25 mL of 2M HNO_3 at 90°C for few hours. During this time, aliquots of 0.5 mL were regularly taken off and replaced by the same volume of fresh nitric acid solution to maintain a constant volume of solution. Depending on the dissolution conditions, i.e. on the basis of the concentration of released uranium, the aliquots were diluted with 0.2 M HNO_3.

In order to study the impact of the nitric acid concentration, pellets were placed in contact with 25 mL of 0.1 to 4M HNO_3 at room temperature. Nitric acid solutions were prepared from analytical grade reagents (supplied by Sigma or Fisher). The leaching solution was continuously renewed using a peristaltic pump in order to avoid any saturation process. At the outlet of the dissolution reactor, the solution passed through a 0.45 µm filter before being regularly sampled using an automatic fraction collector. The flow rate varied from 1 to 5 $mL.h^{-1}$, depending on the nitric acid concentration, in order to allow the determination of the elementary concentrations in the outflow by ICP-AES measurements. The intensity of the peaks was recorded at λ = 279.394 nm, 367.007 nm and 409.014 nm for uranium and at λ = 283.231 nm, 283.730 nm and 401.913 nm for thorium to avoid any interference between the studied elements.

As already described in previous works, the progress of the dissolution reaction of a solid phase is monitored through the determination of the normalized mass loss $N_L(i,t)$ ($g.m^{-2}$) [29], which is defined as:

$$N_L(i,t) = \frac{m_i(t)}{f_i \times S} \quad (2)$$

where, $m_i(t)$ (g) is the mass of element i measured in solution at time t, S (m^2) is the surface area of the solid in contact with the solution and f_i ($g.g^{-1}$) is the mass ratio of the element i in the solid. The surface area of the sample is defined as:

$$S = S_{SA} \times m_0 \quad (3)$$

where S_{SA} ($m^2.g^{-1}$) denotes the initial specific surface area of the solid measured by the SESAM method, and m_0 (g) is the initial mass of solid introduced in the system.

The normalized dissolution rate, $R_L(i)$ ($g.m^{-2}.d^{-1}$), is defined as the time-derivative of the normalized mass loss, *i.e.*:

$$R_L(i) = \frac{\mathrm{d}\, N_L(i)}{\mathrm{d}t} = \frac{1}{f_i \times S} \times \frac{\mathrm{d}\, m_i}{\mathrm{d}t} \quad (5)$$

The use of Equation (5) can be considered as acceptable as soon as the surface area remains constant. This assumption was found to be reasonable and led to an error lower than the experimental uncertainties for a mass loss that does not exceed 5 % of the initial mass of the solid sample [28]. The normalized dissolution rate in a stirred flow-through reactor is obtained when the steady state is reached from the following mass balance expression:

$$\mathrm{R_L(i)} = \frac{\mathrm{d}}{\mathrm{S \times M_i \times f_i}} (\mathrm{C_i} - \mathrm{C_i^{in}}) \quad (6)$$

where d ($L.d^{-1}$) is the flow rate and C_i^{in} (M) is the elementary concentration of i in the inflow, which usually equals zero. The elementary concentrations at steady state C_i (M) were determined by averaging the values measured by ICP-AES.

The dissolution was qualified as congruent when all the normalized dissolution rates were identical (i.e. when all the elements were released with the same ratios than the stoichiometry of the material or more generally when $1/3 < R_L(i)/ R_L(j) < 3$) [30]. For a congruent dissolution, the $R_L(i)$ values determined from the release of each constitutive element in solution are then equal to the dissolution rate of the solid.

III. RESULTS AND DISCUSSION

3.1. Materials features

The various samples prepared by the protocols I to V described above, including both oxalate precursors and the final $Th_{0.5}U_{0.5}O_2$ oxides, were first characterized by SEM. Figure 1 shows selected pictures for each series. The hydrothermal synthesis of mixed oxalates (method I) led to the formation of large agglomerates of about 100 µm in length, whereas the direct precipitation of the same compounds at 60°C produced much smaller grains (about 3-5 microns), presenting the characteristic square-plate habit of the tetravalent actinides oxalates dihydrate. The thermal conversion of these powders into thorium-uranium oxide solid solutions after heating at 500°C under Ar/H_2 (4%) did not modify the starting morphology and only resulted in a slight isotropic decrease of the grains size. Once again, this observation is in very good agreement with literature concerning actinides oxalates since pseudomorphic conversion when heating was frequently described for such kinds of compounds [31]. Moreover, if a clear modification of the sample morphology can be operated depending on the precipitation mode considered (i.e. hydrothermal conditions or direct precipitation), the introduction of an additional mechanical grinding step mostly erases this effect, resulting in all cases in the formation of sub-micrometric grains as viewed in Figure 1. Nevertheless, whatever the final morphology of the oxides, X-EDS analyses confirmed the formation of homogenous solid solutions for protocols I and II with x = 0.48(2) and 0.49(2), respectively.

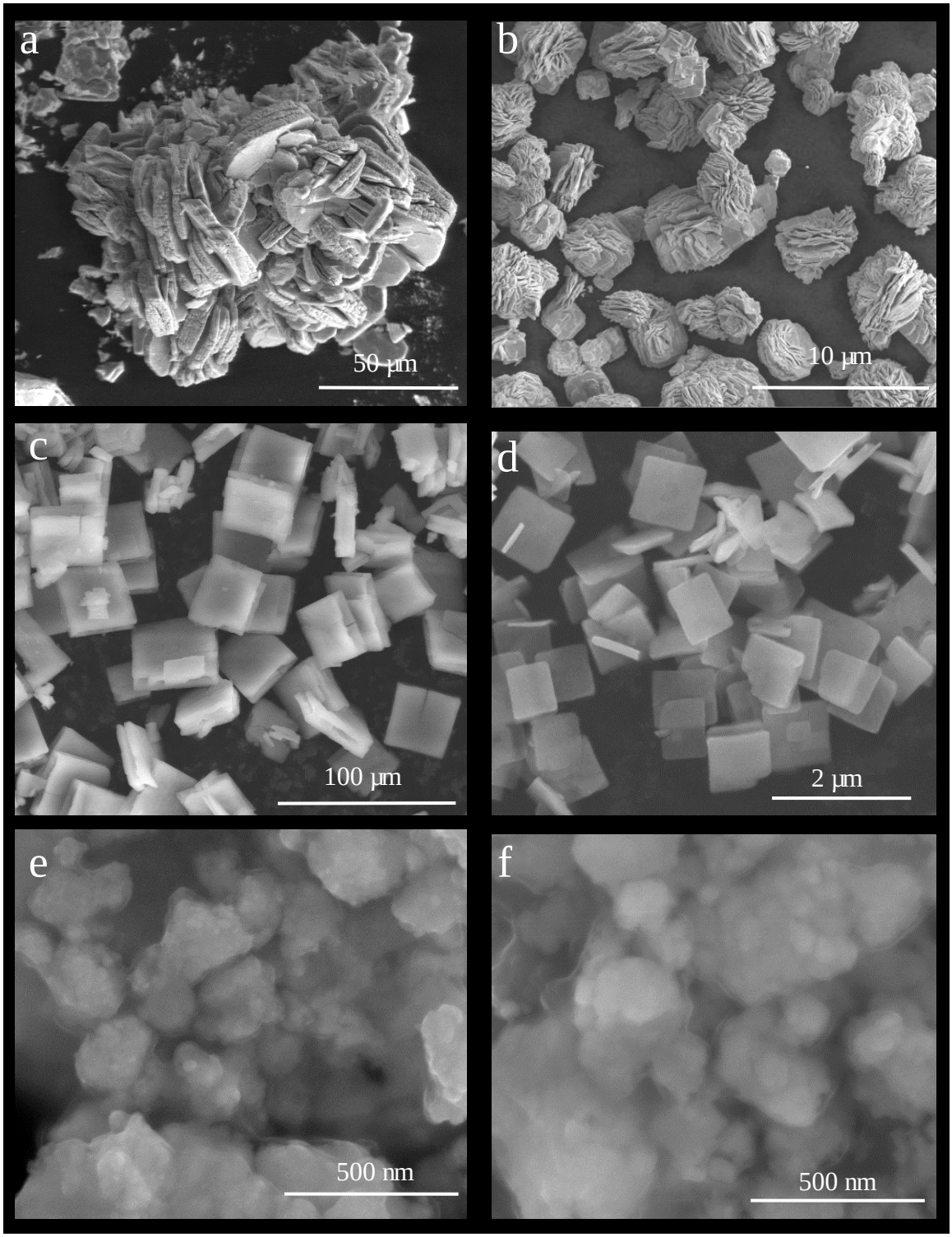

Figure 1. Selected SEM micrographs recorded for raw series of a) I-$Th_{0.5}U_{0.5}(C_2O_4)_2.2H_2O$; b) I-$Th_{0.5}U_{0.5}O_2$; c) II-$Th_{0.5}U_{0.5}(C_2O_4)_2.2H_2O$; d) II-$Th_{0.5}U_{0.5}O_2$ and ground series of e) II-$Th_{0.5}U_{0.5}(C_2O_4)_2.2H_2O$ and f) II-$Th_{0.5}U_{0.5}O_2$.

3.1.1 Powder X-Ray Diffraction

The synthesized oxalate precursors prepared following the protocols I and II were found to be pure and monophasic, their pattern being in good agreement with the monoclinic structure (C2/c space group) reported in the literature [25]. Combined with the X-EDS results, these samples can thus be attested as $Th_{0.5}U_{0.5}(C_2O_4)_2.2H_2O$ solid solutions. The refined unit cell parameters (Table 1) are also consistent with this assumption as the volumes determined (846.70(3) and 845.17(7) $Å^3$) lies between that of the $Th(C_2O_4)_2.2H_2O$ (859.04(9) $Å^3$) and $U(C_2O_4)_2.2H_2O$ (838.34(9) $Å^3$) end-members [32].

Table 1. Refined unit cell parameters for the synthesized $Th_{1-x}U_x(C_2O_4)_2.2(H_2O)$ compounds.

	x **(calc)**	***x*** **(EDS)**	**a (Å)**	**b (Å)**	**c (Å)**	**β (°)**	**Volume ($Å^3$)**
I	0.50	0.48(1)	10.3917(2)	8.4520(2)	9.6390(2)	90.37(1)	846.70(3)
II	0.50	0.49(2)	10.4328(3)	8.5047(5)	9.5257(6)	90.39(1)	845.17(7)
End-members	0	0	10.4485(5)	8.5145(8)	9.6612(1)	90.59(1)	859.46(13)
	1	1	10.459(2)	8.5057(4)	9.4266(4)	90.24(1)	838.60(6)

The thermal conversion of the uranium-thorium bearing oxalate powders led systematically to the formation of pure $Th_{0.5}U_{0.5}O_2$. From Figure 2, the introduction of a grinding step does not affect the structural properties of the final oxides prepared through protocols I and II and in both cases it leads to the formation of a solid solution as shown by the unit cell parameters reported in Table 2. Conversely, when processing through oxalate precursors mixing (method III), an additional grinding step is required to yield a single phase $Th_{0.5}U_{0.5}O_2$ solid solution, a mixture of oxides being obtained otherwise. In the case of methods IV and V, a degradation of the cationic homogeneity is systematically detected and a mixture of oxides is observed. Moreover, for the samples prepared at 500°C the crystallites size ranged from 3 to 5 nm whereas it reached 17-25 nm for those prepared at 1000°C (Table 2). However, this difference in the crystallites size and in the morphology of the powder did not affect significantly the specific surface area which ranged from 7 to 12 m^2/g.

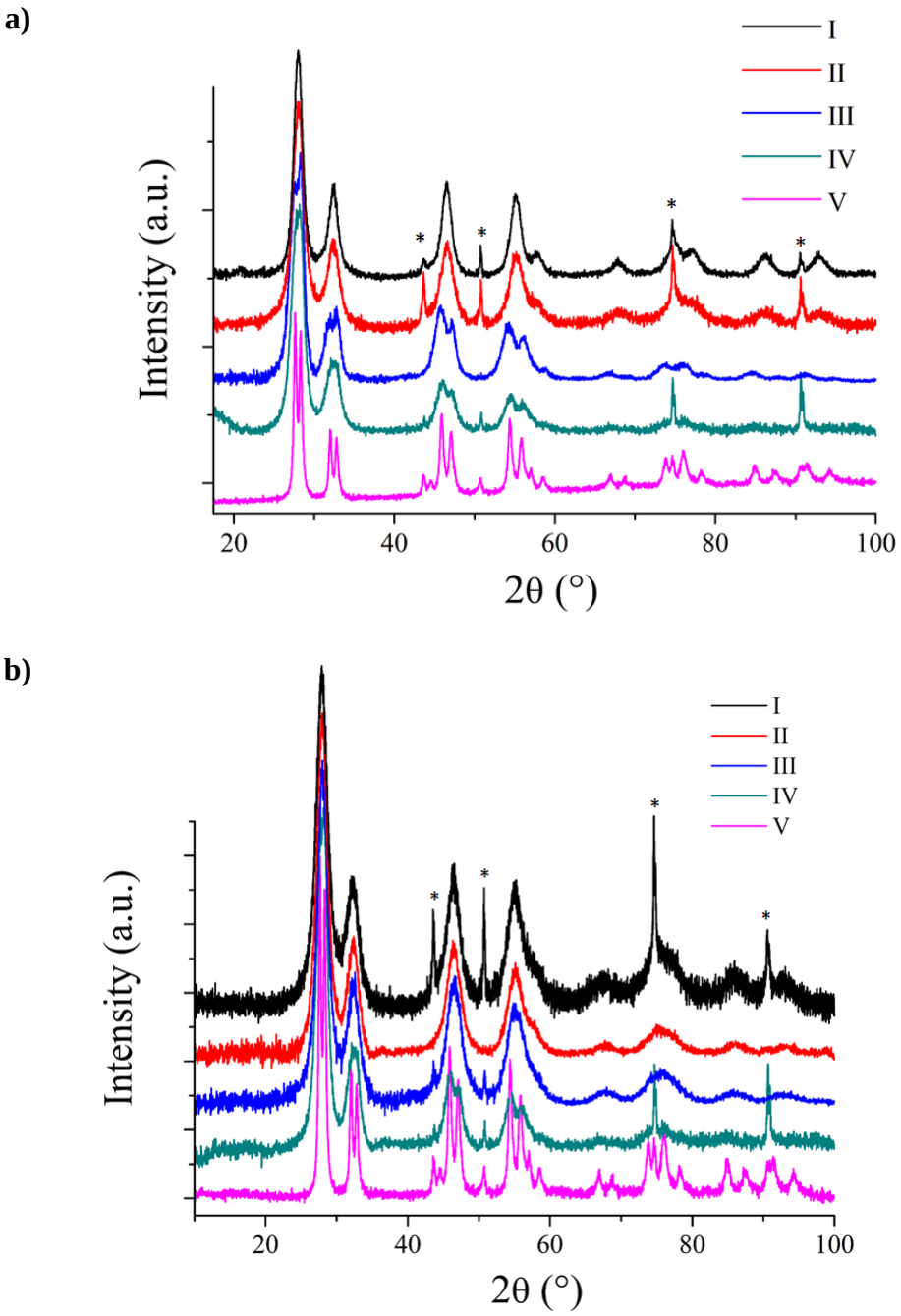

Figure 2. PXRD patterns collected for $Th_{0.5}U_{0.5}O_2$ raw (a) and ground (b) samples (*: XRD peaks of the sample holder).

Table 2. Refined unit cell parameters and average crystalline size obtained for the mixed oxides $Th_{1-x}U_xO_2$ (raw and ground series)

Method	x (calc)	x (EDS)	a (Å)	Volume (Å^3)	Average crystallites size (Å)
Raw series					
I	0.50		5.5268(1)	168.82(1)	48 ± 4
II	0.50	0.49(2)	5.5222(3)	168.40(1)	33 ± 6
IV	0	0	5.6102(4)	176.58(2)	38 ± 2
	1	1	5.4405(3)	161.03(1)	56 ± 14
V	0	0	5.6003(1)	176.64(1)	139 ± 29
	1	1	5.4712(1)	163.77(1)	238 ± 54
Ground series					
I	0.50	0.48(1)	5.5343(3)	169.5(2)	28 ± 5
II	0.50	0.49(2)	5.5264(5)	168.78(2)	38 ± 8
III	0.5	0.48(2)	5.5349(4)	169.56(2)	33 ± 3
IV	0	0	5.6078(3)	176.36(2)	44 ± 4
	1	1	5.4434(3)	161.29(1)	51 ± 4
V	0	0	5.5974(1)	175.38(1)	177 ± 38
	1	1	5.4679(1)	163.48(1)	253 ± 15

3.2. Sintering and characterizations of pellets

In order to evaluate the impact of the heterogeneities in the cation distribution induced by the various protocols applied during the preparation of the powders, dilatometric experiments were undertaken up to 1500°C. Figure 3 evidences drastic differences in the sintering process of the powders depending on their origin. First, the solid solutions obtained from the initial precipitation of $Th_{0.5}U_{0.5}(C_2O_4)_2.2H_2O$, either under hydrothermal conditions or in an open vessel, exhibit a two-step shrinkage already depicted in the literature for such compounds [33, 34]. The first stage lying between 500 and 1100°C was then assigned to sintering and grain growth phenomena within the square-shaped agglomerates described previously in section 3.1. Conversely, the second stage, which is marked by a significant decrease of the pellet thickness, was correlated to the sintering between the agglomerates and led to the densification of the sample. This process was found to be complete as soon as from

1200°C, which appears very low in comparison to the temperatures generally reported in the literature for the sintering of actinide dioxides [35].

The powders obtained through mixing of oxalate end-members or of oxides coming from oxalate conversion at 500°C presented a very similar behavior. In these cases, the first shrinkage stage observed between 500 and 700°C was assigned to grain growth phenomena, which are probably favored by the grinding step performed to homogenize the mixture of the powders. This process probably occurs through surface diffusion, known to present a lower activation energy in comparison to volume and grain boundaries diffusion, generally related to densification processes [36]. At higher temperatures, only a weak residual shrinkage was recorded, showing that the sintering capability of the samples was significantly hindered by the use of powder metallurgy processes (*i.e.* mixtures of large sized powders through mechanical grinding followed by shaping and high temperature heat treatment). Such conclusion was even more enlighten by the sample prepared following protocol V, since no shrinkage was noted below 1000°C for this sample. On this basis, it is likely that the heating step led to the homogenization of the distribution of the cations in the system rather than to the densification of the pellet. Indeed, Gabard *et al.* already evidenced the homogenization of cations due to interdiffusion processes in thoria-based materials [37] while the use of heterogeneous powder mixture is known to delay significantly the sintering of mixed oxides ceramics [16, 38].

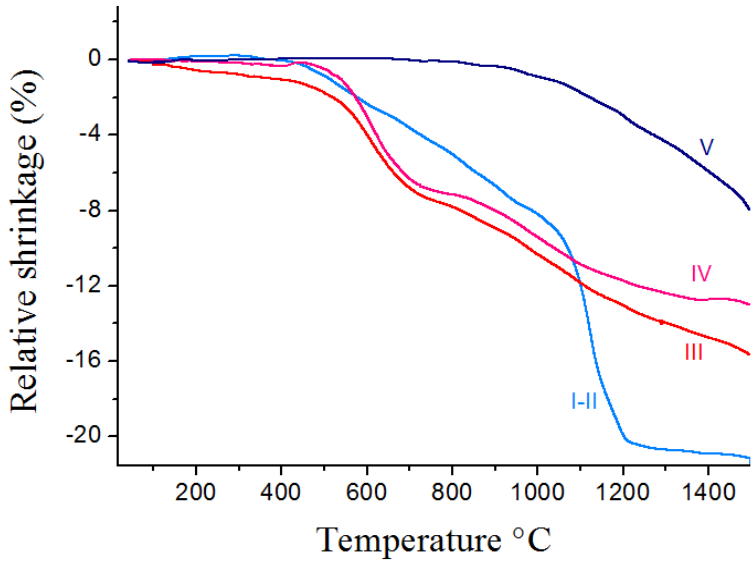

Figure 3. Dilatometric curves recorded during the sintering of raw powders using the five ways of preparation: I-II (light blue), III (red), IV (pink) and V (dark blue).

Beyond the shape of the dilatometric curve, which clearly evidences differences in the sintering mechanisms, the impact of the heterogeneity of cation distribution was directly evidenced by the final linear shrinkage measured after firing at 1500°C. Indeed, this latter reached about 20% for samples prepared by wet chemistry methods, while it was below 10% for protocol V. These differences were also noted on the SEM micrographs recorded at the surface of the various pellets prepared (Figure 4). Indeed, only the powders prepared through wet chemistry methods led to fully densified pellets (i.e. in the 96 – 98 %TD range), which do not exhibit significant amount of open porosity at the surface. For such conditions of preparation, the initial grinding of the samples only led to a modification of the average grain size, which is lowered from about 5 – 10 µm to 1 – 5 µm. As attested by the dilatometric study, the use of powder metallurgy methods generally decreases the final densification state of the pellets, which was generally found between 80 and 90 %TD from geometrical measurements. The ceramics obtained following protocol III (*i.e.* mixture of oxalates) still present the characteristic features of sintered materials, showing the formation of grain boundaries associated to significant grain growth, but also reveal the presence of numerous open pores.

Conversely, all the samples prepared from the mixture of oxide powders led to an incomplete sintering process. More particularly, the micrographs clearly show that the densification only proceeded within the agglomerates, leading to dense zones separated by large pores. Moreover, it is important to note that an additional mechanical treatment of the powders prepared through protocols III to V was not associated to a significant increase of their sintering capability, the final microstructure of the pellets being strongly comparable to their counterparts obtained from raw powders.

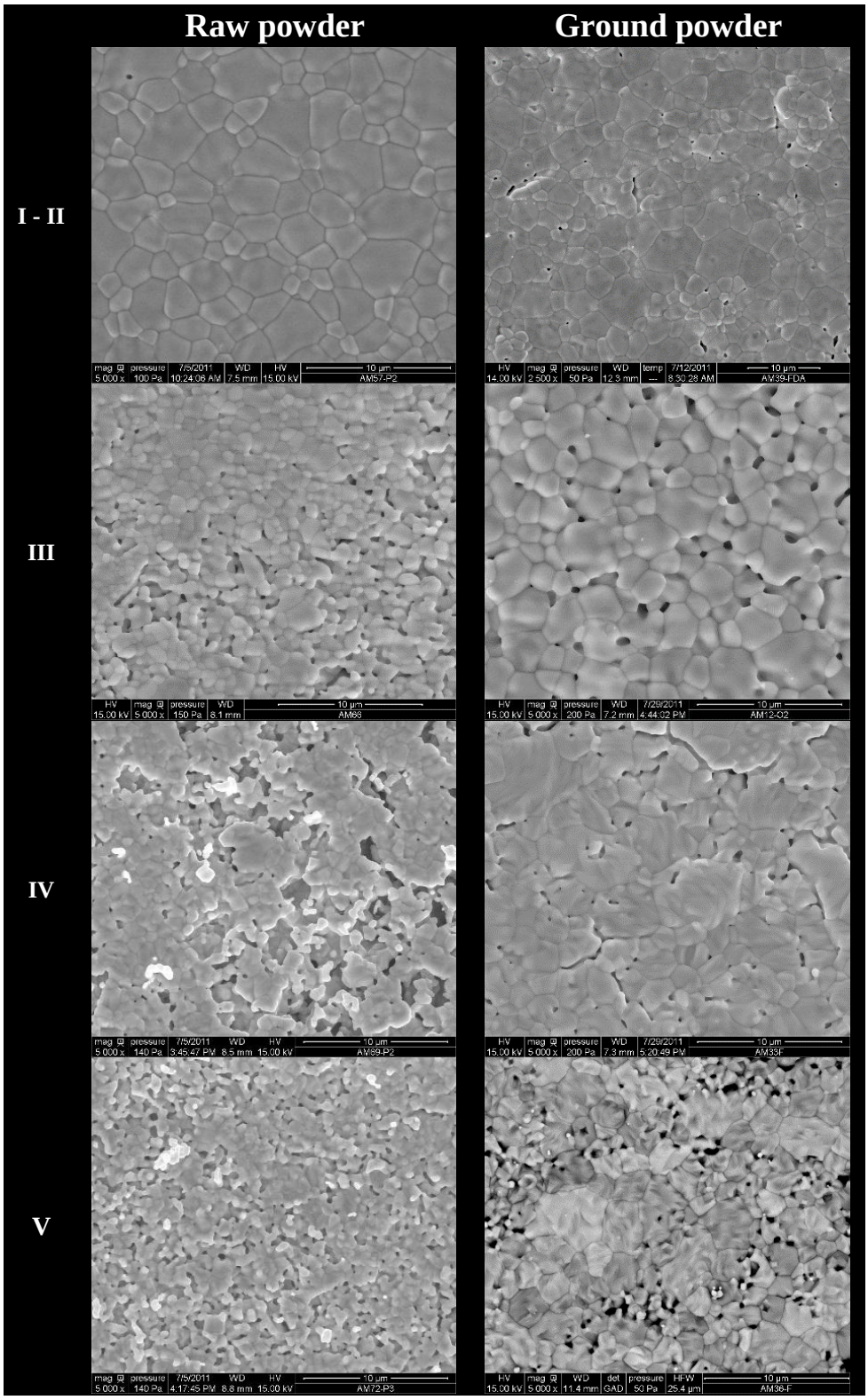

Figure 4. SEM micrographs recorded at the surface of the pellets prepared by using the five protocols after pelletizing then heating for 8 hours at 1500°C under Ar atmosphere

Finally, the surface of the various sintered pellets produced was investigated by the means of X-EDS mapping in order to evaluate the distribution of uranium and thorium. In this aim, the relative deviation regarding to the average chemical composition (illustrated by the uranium incorporation rate in mixed oxide, x) was plotted statistically from the 750000 data points considered (Figure 5). For raw powders series (i.e. without any additional grinding step), two types of distribution were clearly evidenced. The first one was associated to wet chemistry methods of preparation (i.e. protocols I and II) and corresponds to an highly homogeneous composition close to the calculated values. In this case, the FWHM value (Full Width at Half Maximum) was found to be close to 0.11, meaning that most of the data points analyzed led to chemical compositions ranging from $Th_{0.55}U_{0.45}O_2$ to $Th_{0.45}U_{0.55}O_2$. Nevertheless, one must note that for protocol II, a small shoulder corresponding to a limited fraction of uranium-enriched zones was observed. On the other hand, and as expected from the results already compiled in the literature [18, 39, 40], the dry chemistry routes led to heterogeneous samples, illustrated by the dramatically wide aspect of the distribution curve. Indeed, even if a small peak was noticed for compositions closed to $Th_{0.85}U_{0.15}O_2$, the incorporation rate of uranium appeared to be very scattered up to pure UO_2 spots. Also, the absence of data points corresponding to pure ThO_2 allows to get first insights on the homogenization processes, which seem to proceed mainly through the diffusion of uranium in thorium-enriched zones, in good agreement with the values of diffusion coefficients reported in the literature [41, 42].

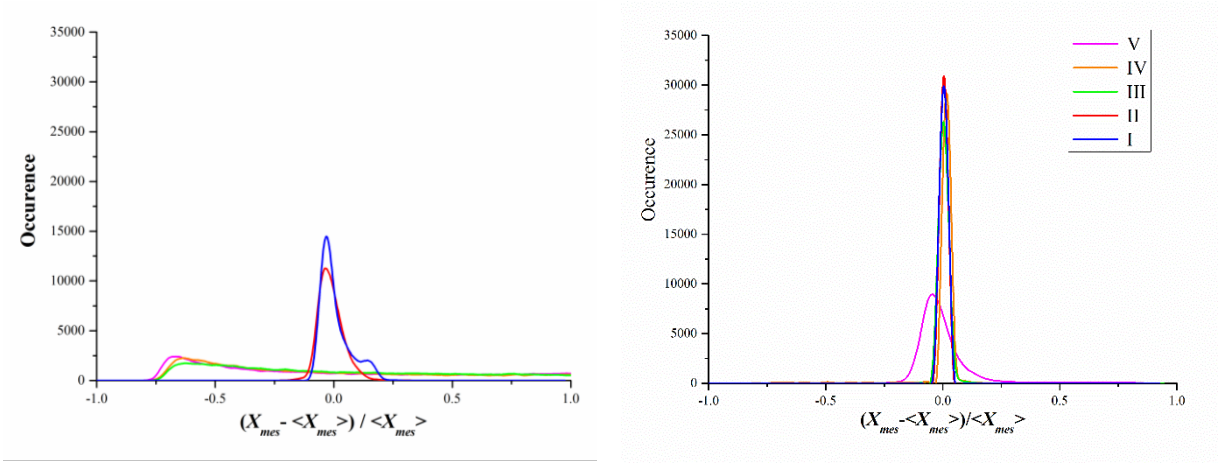

Figure 5. Statistical analysis of the distribution of the cations within $Th_{0.5}U_{0.5}O_2$ sintered samples prepared through the different protocols studied.

Besides, the introduction of an additional mechanical grinding step prior the calcination and sintering of the powders systematically led to the homogenization of the systems. In these conditions, the FWHM values were all in the 0.04 – 0.05 range for protocols I to IV, but remained higher than 0.13 for the sample obtained from the mixture of oxide powders initially fired at 1000°C. Indeed, such a high conversion temperature probably led to low specific surface areas associated with large crystallites, which hinder the reactivity of the powders.

3.3. Behavior of the pellets during dissolution tests : macroscopic description

In order to underline the impact of the cationic distribution on the chemical durability of thorium-uranium(IV) mixed oxides, dissolution experiments were performed on the $Th_{0.5}U_{0.5}O_2$ sintered samples prepared according to the five different protocols described previously. In order to avoid any impact from other parameters on the dissolution of the materials, preliminary calcination step, shaping of the powders and sintering (T = 1500°C, t = 8 hours, Ar atmosphere) remained unchanged for all the samples prepared.

Dissolution tests were undertaken in 2 M HNO_3 at 90°C. The evolution of the normalized mass losses are plotted in Figure 6 and in Figure 7, while the corresponding normalized dissolution rates are gathered in Table 3.

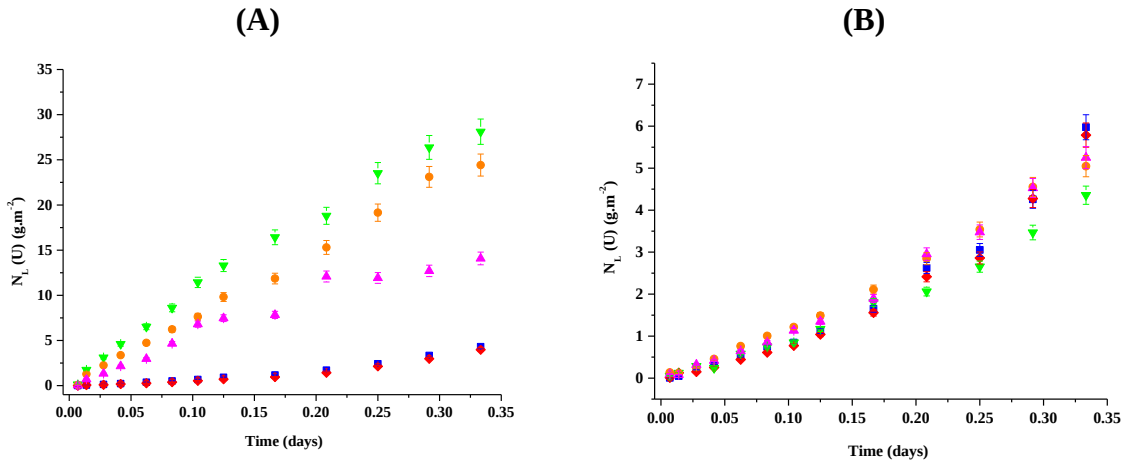

Figure 6. Evolutions of normalized weight losses $N_L(U)$ observed during the dissolution in HNO_3 2M at 90°C of $Th_{0.5}U_{0.5}O_2$ sintered samples prepared following protocols I (■), II (♦), III (▼), IV (●) and V (▲) without (A) or with (B) preliminary grinding step.

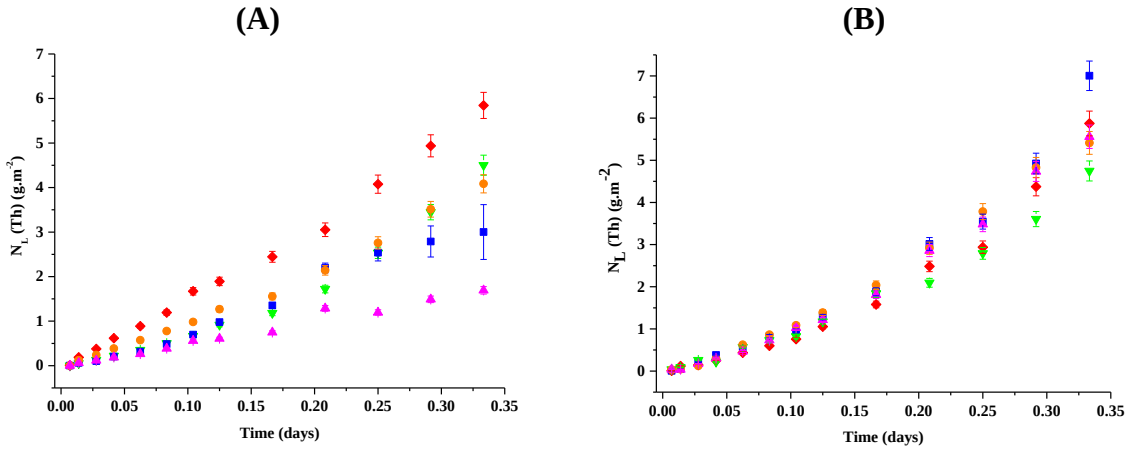

Figure 7. Evolutions of normalized weight losses N_L(Th) observed during the dissolution in HNO_3 2M at 90°C of $Th_{0.5}U_{0.5}O_2$ sintered samples prepared following protocols I (■), II (♦), III (▼), IV (●) and V (▲) without (A) or with (B) preliminary grinding step.

When no milling step was performed before the sintering of the pellets, the normalized dissolution rates calculated from the release of uranium were found to increase by around one order of magnitude when shifting from wet chemistry methods (protocols I and II) to powder metallurgy processes (III – V). This observation appears in very good agreement with the results obtained from the X-EDS mappings (see Figure 5), which suggests a much improved cationic distribution when starting from co-precipitated oxalic precursors. Moreover, the dissolution of the oxide ceramics was found to be congruent for these two preparation methods (I and II) since the congruency ratio, $r = R_{L,0}(U)/ R_{L,0}(Th)$, was close to 1.

However, even if the $R_{L,0}$(Th) appeared to be only slightly modified when considering dry chemistry routes of preparation, the congruency ratio r appeared to increase significantly ($r > 3$) for synthesis protocols III, IV and V, which underlines the preferential dissolution of uranium-enriched zones in the material. Indeed, we recently reported the dissolution of powdered samples of $Th_{1-x}U_xO_2$ solid solutions by varying several parameters such as temperature, chemical composition, leachate acidity, … [43]. Conversely to what observed for $Th_{1-x}Ce_xO_2$ solid solutions [44], the chemical composition induces strong modifications of the chemical durability of the leached samples. The chemical durability of $Th_{1-x}U_xO_2$ solid solutions was significantly affected by the uranium mole loading in the samples due to oxidation of tetravalent uranium into uranyl during the dissolution process.

Table 3. Normalized dissolution rates $R_{L,0}(U)$ and $R_{L,0}(Th)$ (in $g.m^{-2}.d^{-1}$) and congruency ratio $r = R_{L,0}(U)/R_{L,0}(Th)$ determined during the dissolution, in 2M HNO_3 and at T = 90°C, of $Th_{0.5}U_{0.5}O_2$ sintered samples prepared following the five synthesis protocols, and with the presence or not of a grinding step prior the sintering step.

Grinding step	Protocol	$R_{L,0}(U)$	$R_{L,0}(Th)$	r
No	*I*	6.9 ± 0.1	6.7 ± 0.2	**1.03 ± 0.05**
	II	5.3 ± 0.2	6.9 ± 0.4	**0.77 ± 0.08**
	III	108 ± 3	15.9 ± 0.5	**6.8 ± 0.4**
	IV	77 ± 3	10.2 ± 0.3	**7.5 ± 0.5**
	V	57 ± 3	4.8 ± 0.2	**11.9 ± 1.2**
Yes	*I*	9.3 ± 0.3	10.5 ± 0.3	**0.89 ± 0.06**
	II	7.6 ± 0.3	7.6 ± 0.3	**1.00 ± 0.08**
	III	8.9 ± 0.4	9.0 ± 0.5	**0.99 ± 0.11**
	IV	12.5 ± 0.4	12.8 ± 0.4	**0.98 ± 0.06**
	V	10.8 ± 0.3	10.4 ± 0.4	**1.04 ± 0.07**

Furthermore, when a grinding step was performed prior the sintering step, the normalized dissolution rates determined from the thorium and uranium releases in solution were found to be very similar (typically between 7.6 and 12.5 $g.m^{-2}.d^{-1}$) whatever the way of synthesis considered. This result corresponds to the significant decrease of the uranium normalized dissolution rates for the samples prepared following protocols III, IV and V (Table 4). As instance, a decrease by a factor of 6 of the normalized dissolution rate was observed for the sample prepared through protocol IV. Once again, these results demonstrate that the application of a preliminary grinding step before the shaping and sintering of the powders enhances the homogeneity of the final solids by limiting the presence of uranium-enriched zones. However, as normalized dissolution rates remained almost unchanged for samples prepared by wet chemistry methods, such a grinding step could be avoided for this king of protocol, limiting the risks of contamination during the handling of radioactive powders.

Table 4. Ratio between the normalized dissolution rates obtained for raw samples $R_{L,0}(i)_{NB}$ and milled samples $R_{L,0}(i)_{B}$ determined during the dissolution in 2M HNO_3 at 90°C of sintered samples of $Th_{0.5}U_{0.5}O_2$ prepared following the 5 protocols.

Protocol	$R_{L,0}(U)_{NB}/R_{L,0}(U)_{B}$	$R_{L,0}(Th)_{NB}/R_{L,0}(Th)_{B}$
I	0.74 ± 0.04	0.64 ± 0.04
II	0.70 ± 0.06	0.91 ± 0.09
III	12 ± 1	1.77 ± 0.16
IV	6.2 ± 0.4	0.80 ± 0.05
V	5.2 ± 0.5	0.46 ± 0.04

In order to underline the behaviour of $Th_{1-x}U_xO_2$ mixed oxides with different distributions of cations, several $Th_{0.25}U_{0.75}O_2$ pellets were dissolved at room temperature in various nitric acid solutions (0.05 M to 4 M HNO_3) and using dynamic conditions in order to avoid any saturation process. The initial normalized dissolution rates $R_{L,0}(Th)$ and $R_{L,0}(U)$ are gathered in

Table 5 and in Table 6 for samples prepared by protocol II and V, respectively. The variations of the congruency ratio, $r = R_{L,0}(U)/ R_{L,0}(Th)$, versus the acidity of the solution are plotted in Figure 8 for the samples prepared following the five protocols.

Table 5. Normalized dissolution rates $R_{L,0}(U)$ and $R_{L,0}(Th)$ (expressed in $g.m^{-2}.d^{-1}$) determined during the dissolution of homogenous $Th_{0.25}U_{0.75}O_2$ pellets (prepared following protocol II) at room-temperature and in various nitric acid solutions.

Acid concentration	**4 M**	**2 M**	**1 M**
$R_L(U)$	$(2.6 \pm 0.1) \times 10^{-1}$	$(1.2 \pm 0.1) \times 10^{-1}$	$(2.5 \pm 0.1) \times 10^{-2}$
$R_L(Th)$	$(2.7 \pm 0.1) \times 10^{-1}$	$(1.1 \pm 0.1) \times 10^{-1}$	$(2.4 \pm 0.1) \times 10^{-2}$
r	**1.0 ± 0.1**	**1.0 ± 0.1**	**1.0 ± 0.1**
Acid concentration	**0.5 M**	**0.05 M**	
$R_L(U)$	$(4.8 \pm 0.1) \times 10^{-3}$	$(4.1 \pm 0.1) \times 10^{-4}$	
$R_L(Th)$	$(4.7 \pm 0.1) \times 10^{-3}$	$(5.9 \pm 0.1) \times 10^{-4}$	
r	**1.0 ± 0.1**	**0.7 ± 0.1**	

Table 6. Normalized dissolution rates $R_{L,0}(U)$ and $R_{L,0}(Th)$ (expressed in $g.m^{-2}.d^{-1}$) determined during the dissolution of heterogeneous $Th_{0.25}U_{0.75}O_2$ pellets (prepared following protocol V) at room-temperature and in various nitric acid solutions

Acid concentration	4 M	2 M	0.5 M	0.1 M
$R_L(U)$	$(8.9 \pm 0.1) \times 10^{-1}$	$(2.1 \pm 0.1) \times 10^{-1}$	$(1.8 \pm 0.1) \times 10^{-2}$	$(2.9 \pm 0.1) \times 10^{-3}$
$R_L(Th)$	$(2.5 \pm 0.1) \times 10^{-1}$	$(7.1 \pm 0.1) \times 10^{-2}$	$(8.9 \pm 0.1) \times 10^{-3}$	$(1.8 \pm 0.1) \times 10^{-3}$
r	**3.6 ± 0.1**	**3.0 ± 0.1**	**2.0 ± 0.1**	**1.6 ± 0.1**

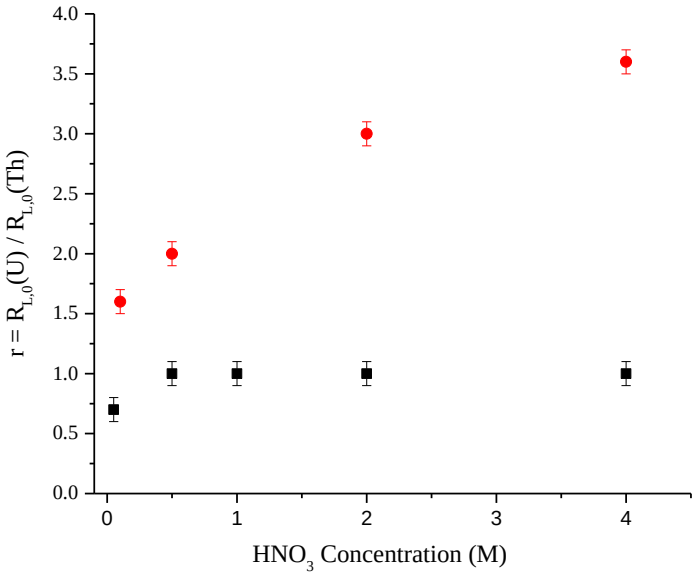

Figure 8. Variation of the congruency ratio, $r = R_{L,0}(U) / R_{L,0}(Th)$, versus the acid concentration, obtained during the dissolution of homogenous (■) and heterogeneous (●) sintered samples of $Th_{0.25}U_{0.75}O_2$ et room temperature

The results obtained for the heterogeneous compound show that the congruency ratio is strongly dependent on the solution acidity. Indeed, this ratio increases from 1.6 (in 10^{-1}M HNO_3) to 3.6 (in 4M HNO_3), thus suggesting that the dissolution is incongruent (

Table 6). This result can be explained by the oxidation of uranium (IV) to uranium (VI), which is much more pronounced when the nitrate concentration of the medium increases [43]. Thus, uranium-enriched zones are more quickly dissolved when the nitric acid concentration is higher than 0.5M. Conversely, uranium-depleted areas retain their refractory character, leading to a clearer difference between uranium-enriched and uranium-depleted zones within

the material. Consequently, the release of uranium in solution is much more important, suggesting the existence of an incongruent dissolution from a macroscopic point of view.

3.4. Behavior of the pellets during dissolution tests: evolution of solid/liquid interface during dissolution test of a heterogeneous $Th_{0.5}U_{0.5}O_2$

In order to better analyze the incongruent character of the dissolution of heterogeneous $Th_{0.5}U_{0.5}O_2$ samples, the solid/liquid interface evolution was monitored by *in operando* ESEM observations during the dissolution of a $Th_{0.5}U_{0.5}O_2$ pellet prepared following the protocol (IV), at room temperature and in 2M HNO_3 (Figure 6). Indeed, such samples can present local heterogeneities in terms of composition which can alter the determination of the normalized dissolution rates.

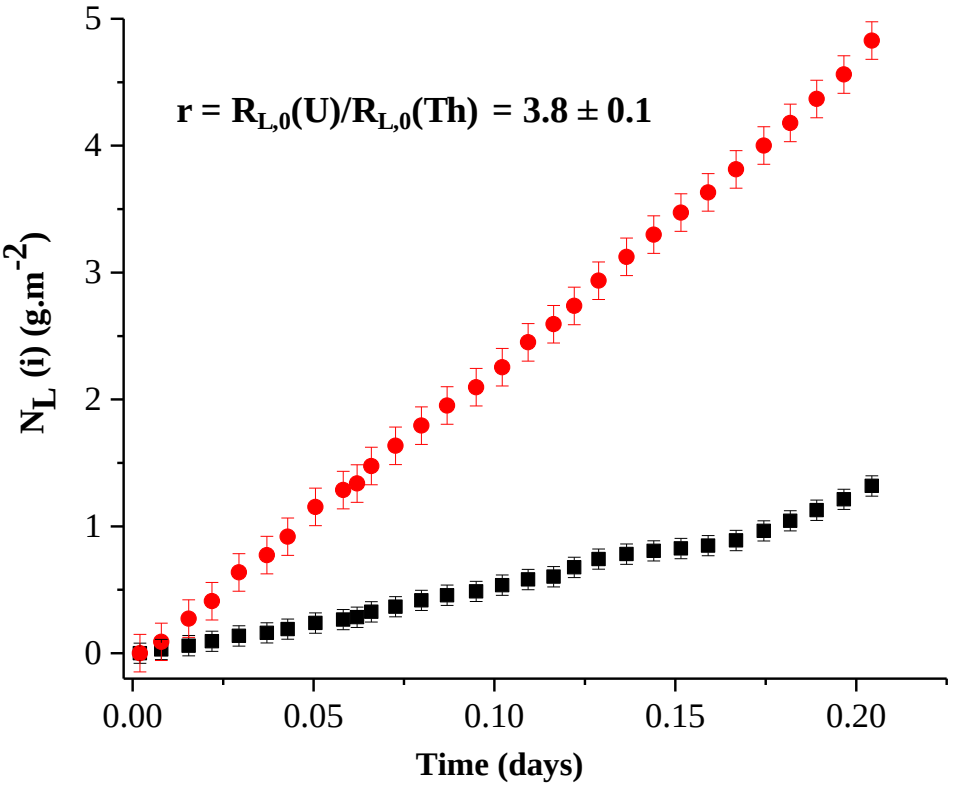

Figure 9. Evolution of normalized weight losses N_L (U) (●) and N_L (Th) (■) observed during the dissolution of heterogeneous $Th_{0.5}U_{0.5}O_2$ sintered samples in HNO_3 2M at room temperature.

From the data plotted on Figure 9, the normalized dissolution rates were found to 6.1 ± 0.1 $g.m^{-2}.d^{-1}$ and 23.4 ± 0.1 $g.m^{-2}.d^{-1}$ for thorium and uranium, respectively, leading to a

congruency ratio $R_L(U) / R_L(Th)$ of 3.8 ± 0.1. Based on this observation, one could conclude on the incongruency in the elemental releases, as previously reported. Apparently, this behavior could result from the presence of fluctuations in terms of cationic distribution within the pellet submitted to dissolution. In order to confirm this assessment, the reactive surface was then evaluated by ESEM at different dissolution stages. With this objective, ESEM pictures were taken on the same selected zone for dissolution times of 0, 3 and 5 hours. The associated BSE micrographs were binarized using the Fiji software to determine the surface area of the altered zones. The results are given in Figure 10 whereas the associated extracted data are gathered in Table 7.

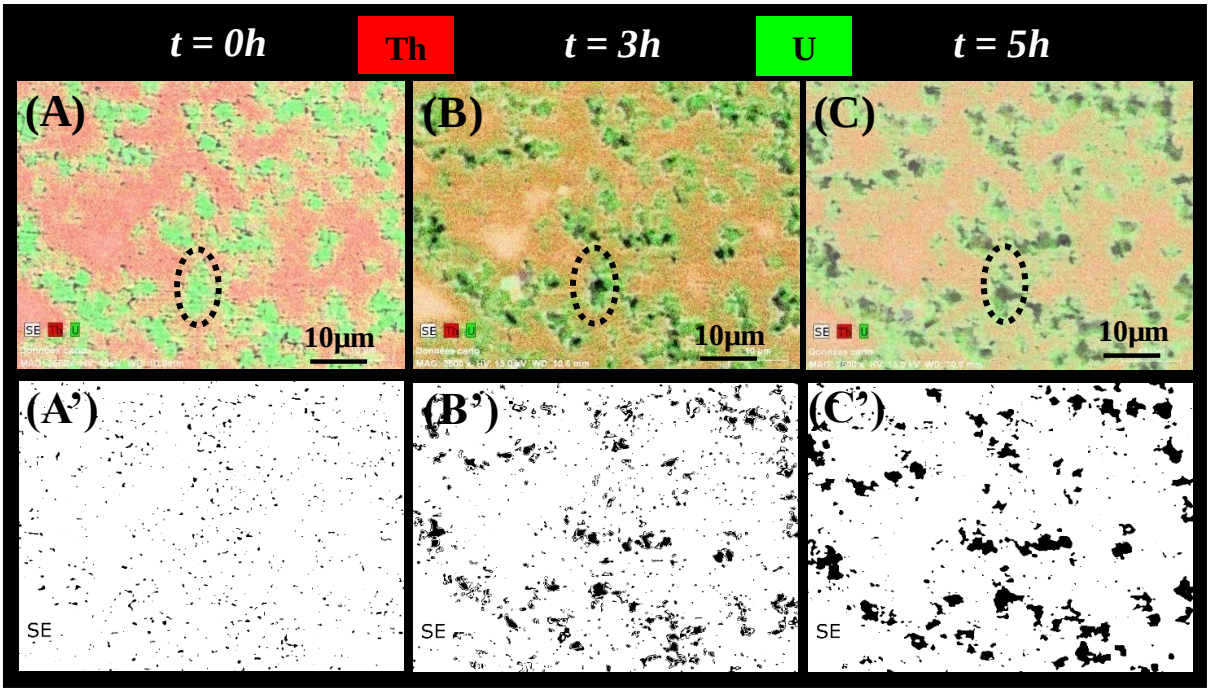

Figure 10. X-EDS hyper-maps showing the evolution of the solid/liquid interface of the pellet during the dissolution experiments at different times (0h (A), 3h (B) and 5h (C)) and the associated binarized BSE micrographs (A', B' and C').

Table 7. Data extracted from the analysis of X-EDS hyper-maps obtained by the X-EDS hyper-maps treatment

Time (hours)	Th (mol.%)	U (mol.%)	x_U	x_{Th}	Dissolved zones %	x_U in dissolved zones
0	19.84	13.50	0.40	0.60	1.9	
3	21.25	12.08	0.36	0.64	7.4	0.77
5	22.12	11.21	0.34	0.66	10.6	0.79

From the analyses of the hyper-maps, evolution of the reactive surface is observed, especially in terms of topography and chemical composition. Indeed, uranium-enriched zones are dissolved preferentially, thus underlining the significant impact of the cationic heterogeneity on the chemical durability of the pellet. Moreover, from the data reported in table 7, it is also possible to evaluate the chemical composition of the altered zones as follows:

$$xU\ (altered\ zones) = 100 \times \frac{\Delta(xU)_t}{\Delta(\%\ altered\ zones)_t} \qquad (7)$$

From this calculation, it appeared that the composition of the dissolved zones equals x_U = 0.78 which agrees with the ratio between cation releases in solution ($r(t) = C_{U(t)} / C_{Th(t)}$ = 4.3). Indeed, making the assumption that both elements are released congruently from dissolved uranium enriched zones, the chemical composition of such zones would be $Th_{0.21}U_{0.79}O_2$ solid solution.

In order to take in account then correct this bias, one must consider the chemical composition of the dissolved zones. Consequently, the parameter f_i ($g.g^{-1}$) (mass ratio) was changed to 0.21 and 0.79 for Th and U, respectively. The evolution of the normalized dissolution weight losses obtained from this correction are plotted in Figure 11.

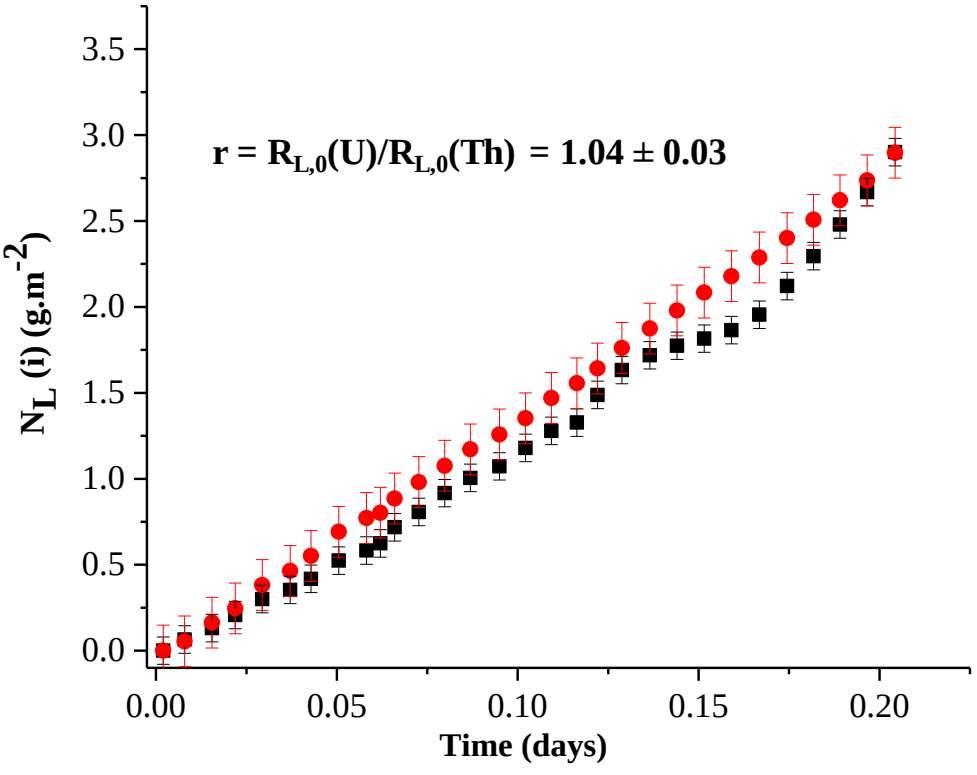

Figure 11. Evolutions of normalized weight losses N_L (U) (●) and N_L (Th) (■) observed during the dissolution of heterogeneous $Th_{0.5}U_{0.5}O_2$ sintered samples in HNO_3 2M at room temperature after being corrected by the real mass ratio of the element *i* in the solid.

As it was expected, the normalized dissolution rates of both elements become very closed ($R_{L,0}(U) = 14.1 \pm 0.1$ g.m^{-2}.d^{-1} and $R_{L,0}(Th) = 13.5 \pm 0.3$ g.m^{-2}.d^{-1}), with a congruency ratio, $R_{L,0}(U)/R_{L,0}(Th)$, of 1.04 ± 0.03 in agreement with the congruent dissolution within the less durable zones. It is thus important to note that such kinds of normalization, required to obtain comparable results in terms of composition and reactivity, leads to satisfactory results for homogeneous compounds. On the contrary, its application can be limited for materials showing chemical heterogeneities in terms of cationic distribution. Thus, it can sometimes induce bias leading to misinterpretation of the data. This point becomes very important to consider in case of materials showing strong heterogeneity that is the case for spent nuclear fuel [45-47], hence the uranium enriched areas could be dissolved quickly the other zones owing to its oxidation.

Conclusion

Five different protocols of synthesis were set up in order to prepare $Th_{0.5}U_{0.5}O_2$ ceramics with different characteristics in terms of cationic distribution, going from the most homogeneous solid solutions obtained through oxalic precipitation to the least, prepared by powder metallurgy from mixture of thorium dioxide and uranium dioxide.

Clear differences were observed when performing the sintering of the powders depending on their origin. A classic two-step shrinkage composed by grain growth phenomena within the square-shaped agglomerates followed by sintering between theses agglomerates was observed for samples prepared by grouped or separate oxalate precipitation. Conversely, using powder mixtures only led to a weak residual shrinkage at high temperature, showing that the sintering capability of the samples was decreased by the use of powder metallurgy processes. Such conclusion was even more enlighten by the sample prepared following the protocol with a mixture of oxides heated at 1000°C, since no shrinkage was noted below 1000°C in this case.

SEM micrographs show that the use of wet chemistry routes helped the elaboration of fully densified pellets (i.e. in the 96 – 98 % TD range) with only few quantity of open porosity at the surface. Conversely, the use of powder metallurgy methods decreases the final densification state of the pellets, with values ranging between 80 and 90% TD f. The surface of the sintered pellets prepared was also investigated through X-EDS mapping showing improved homogeneity and expected chemical composition for the samples produced by protocols I and II. On the contrary, heterogeneities in the cation distribution were observed for samples prepared by dry chemistry routes. Nevertheless, the introduction of an additional mechanical grinding step prior sintering can partially correct this bias.

The impact of cationic distribution on the chemical durability of $Th_{0.5}U_{0.5}O_2$ solid solutions was further examined by performing dissolution tests in acidic media. The normalized dissolution rates calculated from the release of uranium were found to increase by around one order of magnitude when shifting from wet chemistry methods (protocols I and II) to powder metallurgy processes (III – V). Moreover, dissolution tests on homogeneous compounds suggest congruent dissolution, which was not the case for heterogeneous samples. However, dissolution became congruent for all the samples when using a grinding step of the powders prior sintering.

In operando monitoring of the solid/liquid interface evolution during dissolution was finally performed by ESEM on heterogeneous $Th_{0.5}U_{0.5}O_2$ sample. For this kind of materials, the use of normalization induces an important bias leading to the misinterpretation of the dissolution data. Indeed, if the macroscopic analysis of the dissolution concluded on incongruent dissolution, the microscopic examinations of the samples during dissolution through operando experiments associated this apparent incongruent dissolution to the preferential dissolution of uranium enriched zones (in which uranium and thorium were dissolved congruently).

To conclude, these results showed that potential chemical heterogeneity in terms of cationic distribution have to be considered very carefully is one wants to better understand the behavior of actinide oxide base ceramics during reprocessing step or long-term storage in the field of underground repository. Especially, this aspect becomes crucial when making association between the strongly refractory ThO_2 (or CeO_2) with the less durable UO_2.

Acknowledgements

The authors would like to thank Johann Ravaux and Renaud Podor (ICSM/L2ME) for performing the SEM experiments. This work also benefited from financial support of the French National Research Agency (ANR project # ANR-08-BLAN-0216) and from the CNRS Interdisciplinary Research Program MaProSu (Matériaux et Procédés de Remplacement/Substitution).

References

[1] M.S. Ichimiya, Y.T., *American Nuclear Society* **90** (2004) 46-47.

[2] W. Hoffelner, *Chimia* **59**(12) (2005) 977-982.

[3] J. Tommasi, M. Delpech, J.P. Grouiller, A. Zaetta, *Nuclear Technology* **111**(1) (1995) 133-148.

[4] C. Sevik, T. Cagin, *Physical Review B* **80**(1) (2009).

[5] I.R. Shein, K.I. Shein, A.L. Ivanovskii, *J. Nucl. Mater.* **361**(1) (2007) 69-77.

[6] M. Lung, Nuclear Science and Technology project report EUR 17771 for the European Commission, 1997.

[7] H.S. Gruppelaar, J.P. ;, (2000).

[8] P. Buisson, Rôle de la distribution des compositions cationiques sur l'aptitude à la dissolution des combustibles MOX Caractérisation de la distribution par diffraction des rayons X sur poudre, Université Grenoble 1, Grenoble, 1999.

[9] B. Arab-Chapelet, S. Grandjean, G. Nowogrocki, F. Abraham, *J Alloy Compd* **444** (2007) 387-390.

[10] R.B. Matthews, N.C. Davies, OSTI Technical Report, DoE, Oak Ridge, TN, 1979.

[11] O. Yildiz, *J. Nucl. Mater.* **366**(1-2) (2007) 266-271.

[12] S. Hubert, K. Barthelet, B. Fourest, G. Lagarde, N. Dacheux, N. Baglan, *J. Nucl. Mater.* **297**(2) (2001) 206-213.

[13] N.K. Mitra, S.S. Mahapatra, A.K. Chattopadhyay, *Journal of the Indian Chemical Society* **60**(5) (1983) 499-501.

[14] N. Hingant, N. Clavier, N. Dacheux, N. Barre, S. Hubert, S. Obbade, F. Taborda, F. Abraham, *J. Nucl. Mater.* **385**(2) (2009) 400-406.

[15] N. Hingant, N. Clavier, N. Dacheux, S. Hubert, N. Barre, R. Podor, L. Aranda, *Powder Technol* **208**(2) (2011) 454-460.

[16] T.R.G. Kutty, P.V. Hegde, J. Banerjee, K.B. Khan, A.K. Sengupta, G.C. Jain, S. Majumdar, H.S. Kamath, *J Nucl Mater* **312**(2-3) (2003) 224-235.

[17] T.R.G. Kutty, P.V. Hegde, K.B. Khan, S. Majumdar, D.S.C. Purushotham, *J Nucl Mater* **282**(1) (2000) 54-65.

[18] M. Durazzo, H.G. Riella, *Advanced Powder Technology Ii* **189-1** (2001) 60-66.

[19] F. Lebreton, D. Prieur, A. Jankowiak, M. Tribet, C. Leorier, T. Delahaye, L. Donnet, P. Dehaudt, *J Nucl Mater* **420**(1-3) (2012) 213-217.

[20] R. Verma, *J Nucl Mater* **120**(1) (1984) 65-73.

[21] G. Heisbourg, S. Hubert, N. Dacheux, J. Ritt, *J Nucl Mater* **321**(2-3) (2003) 141-151.

[22] G. Heisbourg, S. Hubert, N. Dacheux, J. Purans, *J. Nucl. Mater.* **335**(1) (2004) 5-13.

[23] G. Heisbourg, Synthèse, caractérisation, et études cinétique et thermodynamique de la dissolution de ThO_2 et des solutions solides $Th_{1-x}M_xO_2$ (M = U, Pu), Université Paris-Sud-XI, 2003.

[24] H.D. Greiling, K.H. Lieser, *Radiochimica Acta* **35**(2) (1984) 79-89.

[25] N. Clavier, N. Hingant, M. Rivenet, S. Dobbade, N. Dacheux, N. Barre, F. Abraham, *Inorganic Chemistry* **49**(4) (2010) 1921-1931.

[26] C. Frontera, J. Rodriguez-Carvajal, *Physica B-Condensed Matter* **350**(1-3) (2004) E731-E733.

[27] D. Horlait, L. Claparede, F. Tocino, N. Clavier, J. Ravaux, S. Szenknect, R. Podor, N. Dacheux, *Journal of Materials Chemistry A* **2**(15) (2014) 5193-5203.

[28] T. Cordara, S. Szenknect, L. Claparede, R. Podor, A. Mesbah, C. Lavalette, N. Dacheux, *J. Nucl. Mater.* **496** (2017) 251-264.

[29] A.C. Thomas, N. Dacheux, P. Le Coustumer, V. Brandel, M. Genet, *J. Nucl. Mater.* **281**(2-3) (2000) 91-105.

[30] N. Clavier, E.D. de Kerdaniel, N. Dacheux, P. Le Coustumer, R. Drot, J. Ravaux, E. Simoni, *J Nucl Mater* **349**(3) (2006) 304-316.

[31] D. Horlait, N. Clavier, N. Dacheux, R. Cavalier, R. Podor, *Materials Research Bulletin* **47**(12) (2012) 4017-4025.

[32] N. Clavier, N. Hingant, M. Rivenet, S. Obbade, N. Dacheux, N. Barre, F. Abraham, *Inorg Chem* **49**(4) (2010) 1921-1931.

[33] D. Horlait, F. Lebreton, A. Gauthe, M. Caisso, B. Arab-Chapelet, S. Picart, T. Delahaye, *J Nucl Mater* **444**(1-3) (2014) 181-185.

[34] J. Martinez, N. Clavier, T. Ducasse, A. Mesbah, F. Audubert, B. Corso, N. Vigier, N. Dacheux, *Journal of the European Ceramic Society* **35** (2015) 4535-4546.

[35] T. Abe, K. Asakura, Uranium oxide and MOX production, in: R.J.M. Konings, T.R. Allen, R.E. Stoller, S. Yamanaka (Eds.), Comprehensive nuclear materials, Elsevier, Amsterdam, 2012, pp. 393-422.

[36] S.J.L. Kang, Sintering - Densification, Grain Growth & Microstructure, Burlington, 2005.

[37] M. Gabard, Y. Cherkaski, N. Clavier, L. Brissonneau, M.C. Steil, J. Fouletier, A. Mesbah, N. Dacheux, *J Alloy Compd* **689** (2016) 374-382.

[38] T.R.G. Kutty, P.V. Hegde, K.B. Khan, T. Jarvis, A.K. Sengupta, S. Majumdar, H.S. Kamath, *J Nucl Mater* **335**(3) (2004) 462-470.

[39] R. Vauchy, A.C. Robisson, P.M. Martin, R.C. Belin, L. Aufore, A.C. Scheinost, F. Hodaj, *J Nucl Mater* **456** (2015) 115-119.

[40] G. Oudinet, I. Munoz-Viallard, L. Aufore, M.J. Gotta, J.M. Becker, G. Chlarelli, R. Castelli, *J Nucl Mater* **375**(1) (2008) 86-94.

[41] H. Matzke, *J Nucl Mater* **30**(1-2) (1969) 26-&.

[42] K. Ando, Y. Oishi, *J Nucl Sci Technol* **20**(12) (1983) 973-982.

[43] L. Claparede, F. Tocino, S. Szenknect, A. Mesbah, N. Clavier, P. Moisy, N. Dacheux, *J Nucl Mater* **457** (2015) 304-316.

[44] L. Claparede, N. Clavier, N. Dacheux, A. Mesbah, J. Martinez, S. Szenknect, P. Moisy, *Inorganic Chemistry* **50**(22) (2011) 11702-11714.

[45] C. Jegou, R. Caraballo, J. De Bonfils, V. Broudic, S. Peuget, T. Vercouter, D. Roudil, *J. Nucl. Mater.* **399**(1) (2010) 68-80.

[46] J.A. Serrano, J.P. Glatz, E.H. Toscano, D. Papaioannou, J. Barrero, M. Coquerelle, *J. Alloy. Compd.* **271** (1998) 573-576.

[47] M.J. Carrott, P.M.A. Cook, O.D. Fox, C.J. Maher, S.L.M. Schroeder, The chemistry of (U,Pu)O_2 dissolution in nitric acid, in: C. Poinssot (Ed.), Atalante 2012 International Conference on Nuclear Chemistry for Sustainable Fuel Cycles, Elsevier Science Bv, Amsterdam, 2012, pp. 92-97.